NUMERICAL MODEL OF AN ATMOSPHERIC ADAPTIVE OPTICAL SYSTEM.
II. WAVE−FRONT SENSORS AND CONTROL ELEMENTS

V.P.Lukin, F.Yu. Kanev, P.A. Konyaev, and B.V. Fortes

*Institute of Atmospheric Optics,
Siberian Branch of the Russian Academy of Sciences, Tomsk*
Received September 26, 1994

The description of numerical models of adaptive system elements is continued. In particular, a model of the Hartmann sensor and an algorithm for discontinuous phase surface joining are considered. Models of some control elements such as modal and zonal correctors and segmented mirror and two models of flexible mirror (static and dynamic) are also presented.

1. IDEAL DEVICE FOR PHASE RECORDING AND ALGORITHM FOR PHASE SURFACE JOINING

In solving numerically the adaptive optics problems the models of ideal devices operating as optical elements without limitations, characteristic of real physical devices, are often used. A model of an ideal adaptive mirror that enables one to assign arbitrary phase profile, a model of an ideal phase sensor, ideal wave−front conjugation device, and so on are among such models. These models are mathematical abstraction, nevertheless they allow the qualitative (without element−induced limitations) analysis of beam control in the atmosphere to be made.

For an ideal wave−front sensor, the phase distribution is

$\varphi(x, y) = \arg(E)$,

where E is the complex amplitude of a field. Because the argument of a complex number is ambiguous function, this relation may be used only for phase surfaces continuous in the interval $[-\pi; +\pi]$. To remove this limitation, one needs to obtain the total phase of the field

$$\varphi(x,y)=\text{Arg}(E)=\arg(E)+2\pi\, m,\ m= 0, \pm 1, \pm2, \ldots, \qquad (1)$$

i.e., to determine the parameter m (integer) from the condition of the surface continuity at any point of a beam cross section. It should be noted that this condition is invalid in the presence of wave−front dislocations. Otherwise for obtaining the untruncated phase distribution the conventional methods of two−dimensional function reconstruction[1] from its first differences can be used. In the nodes (I, J) of a computation grid these differences are calculated as follows:

$$\Delta_{I,J}^{x} = \arg(E_{I,J}^{*}\, E_{I+1,J}),$$

$$\Delta_{I,J}^{y} = \arg(E_{I,J}^{*}\, E_{I,J+1}),\ I, J = 0, 1, 2, \ldots, N-1, \qquad (2)$$

where N is the size of a grid. It is easy to verify that the discrete Fourier transform (DFT) of the sum of the second differences of the sought−after function

$$\Delta_{I,J}=\Delta_{I,J}^{xx}+\Delta_{I,J}^{yy} = \Delta_{I+1,J}^{x} - \Delta_{I-1,J}^{x} + \Delta_{I,J+1}^{y} - \Delta_{I,J-1}^{y} \qquad (3)$$

is related to its DFT by the relationship

$$\widetilde{\Delta}_{K,L}=\widetilde{\varphi}_{K,L}\, 2[\cos(2\pi K /N)+\cos(2\pi L /N)-2], \qquad (4)$$

where

$$\widetilde{\varphi}_{K,L} = \sum_{I=0}^{N-1}\sum_{J=0}^{N-1} \varphi_{I,J} \exp\left(i\frac{2\pi}{N}[I K + J L]\right),$$

$$\widetilde{\Delta}_{K,L} = \sum_{I=0}^{N-1}\sum_{J=0}^{N-1} \Delta_{I,J} \exp\left(i\frac{2\pi}{N}[I K + J L]\right). \qquad (5)$$

As follows from Eqs. (4) and (5), for the phase reconstruction one needs to compute the inverse DFT of the function

$$\widetilde{\varphi}_{K,L} = \frac{\widetilde{\Delta}_{K,L}}{2\,[\cos(2\pi K / N) + \cos(2\pi L / N) - 2]}, \qquad (6)$$

i.e., the sought−after function is determined as follows:

$$\varphi_{I,J} = \frac{1}{N^{2}} \sum_{K=0}^{N-1}\sum_{L=0}^{N-1} \widetilde{\varphi}_{K,L} \exp\left(- i\frac{2\pi}{N}[I K + J L]\right). \qquad (7)$$

In fact, this algorithm is equivalent to that for a solution of the Poisson equation with periodical boundary conditions in the net−point representation. Different versions of algorithms for phase evaluation from its differences measured with interferometric wave−front sensors solve the same equation. Because of this, the examined algorithm for the total phase reconstruction from the known complex amplitude also can be treated for simulation of an interferometric sensor with its spatial resolution being coincident with the step of a computation grid. In the presence of wave−front dislocations implementation of the above−described algorithm yields smooth phase that does not coincide with the argument of the initial complex amplitude.

2. MODEL OF A HARTMANN SENSOR

In real adaptive optics systems a Hartmann sensor is commonly used for recording of a phase surface. Schematic view of the sensor is depicted in Fig. 1. In accordance with the design of the device the following algorithm was implemented in our numerical model:

1. Setting of the sensor parameters (the number of subapertures and the overall dimensions of the aperture).

2. Separation of a portion falling within a subaperture from the complex amplitude of the field and nullifying the field beyond this subaperture.

　　　　　© 　　　1995　Institute of Atmospheric Optics

3. Multiplication of the separated portion of the field by the apodization function, which has the form

$$\rho(x, y) = \exp\left[-(x^8 + y^8)\,/\,a_0^8\right], \qquad (8)$$

where a_0 is the radius of the subaperture, and the origin of the coordinate system is at the center of the subaperture. This operation is accomplished primarily to diminish the calculational error in solving numerically the propagation problem.

4. Solution of the propagation problem for the field obtained after operations 2 and 3. In this case it is assumed that each subaperture located in the sensor plane focuses the corresponding portion of the field to the image plane 2 (see Fig. 1).

5. Calculation of the local (within the subaperture) shifts of the beam's center of gravity (dx_k, dy_k) from its undisturbed position and calculation of the local tilts $(S_k^x = dx_k\,/F, \; S_k^y = dy_k\,/F$, where k is the serial number of subaperture, and F is the focal length).

Operations from 2 to 5 are executed for each subaperture; after accomplishing this cycle, item 6 is executed.
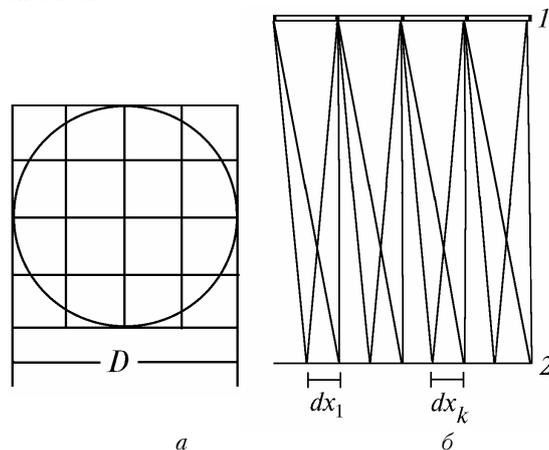
FIG. 1. Schematic view of a Hartmann sensor: aperture of the sensor (a); propagation of beams from the aperture plane (1) to the image plane (2) and separation of local shifts of the beam's center of gravity (b).

6. Assigning the phase surface by a set of Zernike polynomials. Polynomial coefficients are found by the least–squares method from the condition of rms error minimum

$$\Delta^2 = \sum_{k=1}^{N_z} \left\{\left(S_k^x - \sum_{l=1}^{N_z} A_l Z_{lk}^x\right)^2 + \left(S_k^y - \sum_{l=1}^{N_z} A_l Z_{lk}^y\right)^2\right\}. \qquad (9)$$

Here, N_s is the number of subapertures, N_z is the number of polynomials, S_k^x and S_k^y are the local tilts to the x and y axes within the kth subaperture, A_l are polynomial coefficients, and Z_{lk}^x and Z_{lk}^y are the coefficients of the best (in rms meaning) approximation of Z_l polynomial by the linear function $x Z_{lk}^x + y Z_{lk}^y + C_{lk}$ within this subaperture. A solution to the system of equations (9) (i.e., determination of A_l coefficients) means that the phase profile represented by a set of Zernike polynomials is found from the intensity distribution.

The results of numerical experiments on correction for atmospheric distortions of laser beam with the use of the above–described model of the Hartmann sensor are given in Ref. 2.

3. ZONAL CORRECTOR

When constructing the model of zonal corrector, we describe the mirror surface $W(x, y)$ by linear combination of the response functions of actuators

$$W(x, y) = \sum_{l=1}^{N} A_l I_l(x, y), \qquad (10)$$

where N is the number of actuators, A_l is the amplitude of displacement, and I_l is the response function of the lth actuator. The Gaussian form of the actuator response function was assumed.

Approximation of the phase profile $\varphi(x, y)$ by the mirror was performed by the least–squares method, and the coefficients A_l were found from the condition of minimum of the function

$$\Delta^2 = \iint\limits_S \left(\varphi(x, y) - W(x, y)\right)^2 dx\,dy, \qquad (11)$$

where S is the area of the corrector aperture.

Despite the fact that in distinction to the corrector under consideration the form of the response function of a real mirror is not symmetrical and depends on the device geometry (in particular, on the arrangement of the mirror clamping points, configuration of actuators, etc.), in some cases the use of this simplified model enables one to analyze the operation of an adaptive system with satisfactory accuracy.[3]

4. MODAL CORRECTOR

In many theoretical investigations of the adaptive optics system operation the mirror surface is represented as superposition of polynomials (usually Zernike polynomials)[4,5]

$$W(x, y) = \sum_{i=1}^{N_z} A_i Z_i(x, y), \qquad (12)$$

where i is the serial number of polynomial, N_z is the total number of polynomials used to construct the model, A_i is the polynomial coefficient,

$$Z_i(x, y) = R_n^m(x, y) \cos(m\varphi) \text{ for even } i,$$

$$Z_i(x, y) = R_n^m(x, y) \sin(m\varphi) \text{ for odd } i,$$

$$Z_i(x, y) = R_n^m(x, y) \text{ for } m = 0.$$

Here m is the azimuthal frequency, φ is the polar angle, and

$$R_n^m(x,y) = \sum_{j=1}^{(n-m)/2} \frac{(-1)^j (n-j)! \, (x^2 + y^2)^{(n-2j)/2}}{j! \, [(n+m)/2 - j]! \, [(n+m)/2 + j]!}.$$

Using the model under study, a series of investigations on the dependence of the quality of compensation for atmospheric distortions on the number of Zernike polynomials N_z reproduced by a corrector was performed.[6,7] The

calculations accomplished have shown that using modal corrector one can determine the degree of complexity of the phase surface to compensate for distortions under various conditions, as well as to predict approximately the required number of actuators of an adaptive mirror.

5. SEGMENTED MIRROR

The reflecting surface of a segmented mirror is a set of square or hexagonal elements inscribed in a circular aperture (Fig. 2). The numerical model used by us allows the number of segments and degrees of freedom for each element to be changed from one (only shift is set) to three (setting of shift and tilts to two perpendicular axes).
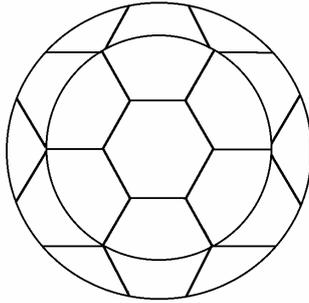
FIG. 2. Segmented mirror with hexagonal elements.

Reproduction of a given phase surface by a segmented mirror was performed by a least–squares method. The accuracy of reproduction and the efficiency of a mirror in the problem of compensation for atmospheric turbulence were considered in Ref. 8.

6. STATIC MODEL OF A FLEXIBLE MIRROR

In numerical experiments the model of a thin homogeneous plate was used as a flexible mirror. Static deformations of the plate were described by equation of biharmonic type[9]

$$D \left(\frac{\partial^4 W}{\partial x^4} + \frac{\partial^4 W}{\partial x^2 \partial y^2} + \frac{\partial^4 W}{\partial y^4} \right) = f(x, y), \qquad (13)$$

where (x, y) are the coordinates in the plane of the plate, D is the cylindrical stiffness, and f is the lateral load. At the points of rigid clamping of the mirror on the frame (at these points the plate cannot be shifted, and deformations appear when tilting the mirror) the boundary conditions can be written in the form:

$$W\big|_{(x_i, y_i)} = \frac{\partial W}{\partial n}\bigg|_{(x_i, y_i)} = 0, \qquad (14)$$

while at the hinged point (where tilting causes no deformations)

$$W\big|_{(x_0, y_0)} = D \left(\frac{\partial^2 W}{\partial n^2} + \sigma \frac{\partial^2 W}{\partial \tau^2} \right)\bigg|_{(x_0, y_0)} = 0. \qquad (15)$$

Here $\partial/\partial n$ and $\partial/\partial \tau$ are the normal and tangential derivatives with respect to the plate plane, and σ is the Poisson coefficient.

Numerical solution of Eq. (13) was found by the finite–element method.[10] By the method, the plate was divided into a set of elements, with the local coordinate system ($O\xi$, $O\eta$) affixed to each element. Deformations of each element were described by the vector

$$\mathbf{w} = \begin{Bmatrix} \xi \\ \varphi \\ \eta \end{Bmatrix},$$

where ξ is the vector of lateral shifts of the element angular points (nodes of a computation grid), φ and η are the vectors of tilt angles with respect to the $O\xi$ and $O\eta$ axes. The vector $\mathbf{w}$ has $3N_e$ components, where N_e is the number of nodes of a grid bounding the element.

The vector of generalized forces $\mathbf{Q}$ is associated with the vector of generalized coordinates $\mathbf{w}$ and has the form

$$\mathbf{Q} = \begin{Bmatrix} \mathbf{P} \\ \mathbf{N} \\ \mathbf{T} \end{Bmatrix},$$

where $\mathbf{P}$ is the vector of shearing forces, and $\mathbf{N}$ and $\mathbf{T}$ are the vectors of deflection moments with respect to the axes of the local coordinate system. The relation between $\mathbf{w}$ and $\mathbf{Q}$, found by the virtual displacement method, has the form[10]

$$[k]\,\mathbf{w} - \mathbf{f} = \mathbf{Q}. \qquad (16)$$

The first term in the left–hand side of Eq. (16) describes the generalized elastic forces ($[k]$ is the stiffness matrix of an element), and the second term describes the external forces. In the right–hand side of Eq. (16), the forces of interaction between the elements are involved. The stiffness matrix $[k]$ is found as an integral of the element potential energy density, in this case the calculation is significantly simplified with limitations on the shape of deflection.[10] For the deflection shape described by a finite power series, the matrix $[k]$ was calculated and presented in Ref. 10.

Taking into account the conditions of element conjugation that follow from the requirement for the continuity of the field of model displacements as a whole and equilibrium of interaction forces between elements, an equation describing static deformation of the whole model can be derived

$$[K]\,\mathbf{W} = \mathbf{F}. \qquad (17)$$

Here $\mathbf{W}$ is the vector of the generalized coordinates of the model, $\mathbf{F}$ is the vector of external forces (both vectors are $3N_m$ − dimensional, where N_m is the number of nodes of the model). The stiffness matrix of the plate $[K]$ also can be found from the conditions of element conjugation, with the order of the matrix being $3N_m \times 3N_m$. Here, it should be emphasized that even for rare grid the operation with the matrix $[K]$ is difficult because of a large number of its elements (this concerns mainly the operations of matrix inversion and data transfer from a hard disk to a random–access memory; the last procedure requires too much time). Thus for the grid 9×9 ($N_m = 81$) the matrix $[K]$ is of order 243×243.

The order of the stiffness matrix $[K]$ can be decreased[10] (reduction is accomplished), and operations with it are simplified if only transverse forces are exerted to the model, i.e., the vector $\mathbf{F}$ included in Eq. (17) is of the form

$$\mathbf{F} = \begin{Bmatrix} \mathbf{P} \\ 0 \\ 0 \end{Bmatrix}.$$

In this case the stiffness matrix components to be multiplied by the zero components of the $\mathbf{F}$ vector can be excluded beforehand. The second reduction of the matrix $[K]$ is carried out using the data on the geometry of actuator arrangement, assuming that at the points where the

actuators are absent external forces do not act on the model. As a result of reduction, the order of the matrix is decreased down to $(N_m - N_{act}) \times N_{act}$ (N_{act} is the number of actuators), i.e., for 9×9 grid the stiffness matrix for a mirror with five actuators would be of the order 76×5, that is, much lower than before the reduction.

7. NUMERICAL MODEL OF A DYNAMIC MIRROR

In the design of an adaptive optical system we have constructed a numerical model of a dynamic mirror enabling us to record the transient processes under deformation of a flexible plate. In this case deflection of the reflecting surface $W(x, y)$ was described by the matrix equation which, as equation (17), was obtained on the basis of the virtual work principle[10]

$$[M]\ddot{W} + [G]\dot{W} + [K]W = F. \tag{18}$$

Here $[M]$, $[G]$, and $[K]$ are the inertia, oscillation damping, and stiffness matrices, respectively. The system of equations (18) was solved by the Runge–Kutta method.[11] The result of the system solution was the dynamic field of lateral shifts of the model nodes, which describes the movements of the plate under the action of given forces. On the basis of this computational scheme the models of a mirror shown in Fig. 3a and b were constructed.
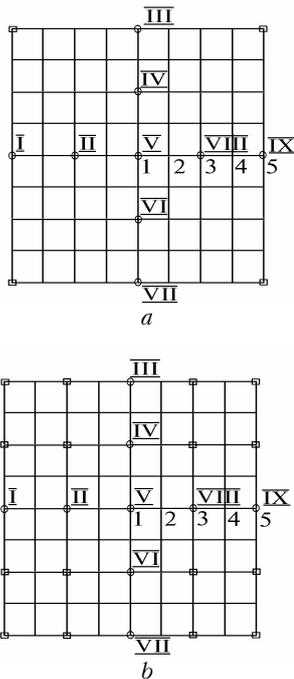
FIG. 3. Models of a flexible dynamic mirror: points of actuator locations (i) and points of mirror clamping on a frame (X) are shown. The serial numbers of points where surface displacements were registered are shown on the models. Actuators are numbered by Roman numerals.

The transient processes illustrated in Figs. 4 and 5 occur when reproducing the given surface by the dynamic corrector. Shown here are the shifts of the points arranged on the mirror radius and the standard deviation $\varepsilon(t)$ of the corrector surface $W(x, y, t)$ from the given profile $\varphi(x, y)$ defined by the formula

$$\varepsilon(t) = \frac{\int\int (\varphi(x, y) - W(x, y, t))^2 \rho(x, y)\, dx\, dy}{\int\int \varphi(x, y)^2 \rho(x, y)\, dx\, dy}, \tag{19}$$

where ρ is the weighting function.

Let us consider the accuracy of parabolic surface approximation by a flexible mirror. The action F was determined by the least–squares method. In Eq. (17) the vector F was introduced as follows (step action):

$$F = \begin{cases} 0, & t \geq 0, \\ (f_1, f_2, \dots, f_n), & t \leq 0, \end{cases} \tag{20}$$

Here f_i are the components of the vector F, and n is the number of actuators.
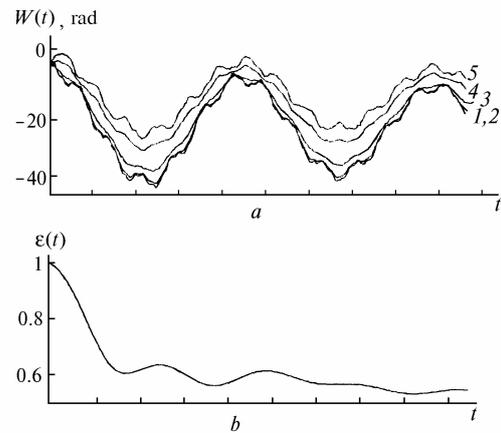
FIG. 4. Transient processes for the model of a mirror shown in Fig. 3a: shifts of reflecting surface at points 1–5 (a) and rms error $\varepsilon(t)$ (b).
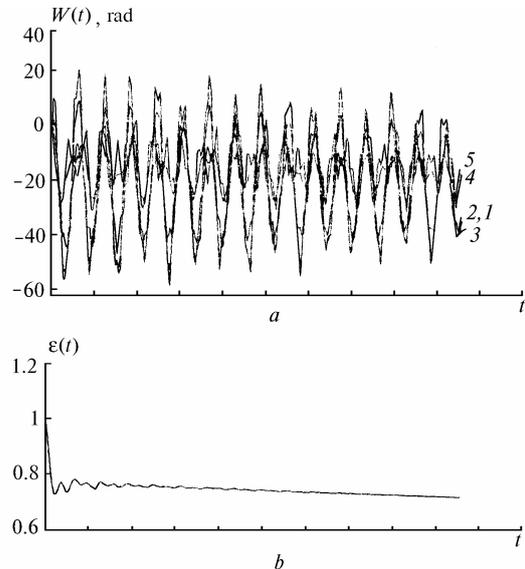
FIG. 5. Transient processes for the model of a mirror shown in Fig. 3b.

Because the damping coefficient was chosen small enough, it is practically impossible to see the damping of surface oscillations in the figures. The amplitude of oscillations of the function ε is small in comparison with its

values, but without damping the accuracy of surface reproduction is insufficient (for a similar static mirror in focusing reproduction ε is 0.10–0.12, see Ref. 12). The data presented demonstrate the increase of frequency with the decrease of the distance between the clamped points and points of force application.
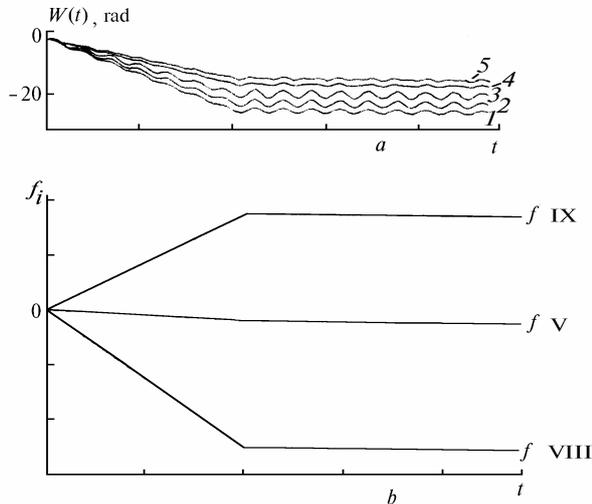
FIG. 6. Oscillations of a mirror surface: (a) transient processes for smooth increase of loading applied to a mirror, for the corrector model shown in Fig. 3b, and (b) variation of forces exerted to the mirror at points V, VIII, and IX.

Earlier we considered the use of dynamic mirror in multidither algorithm.[13] In this case the necessity of signal filtration for separation of variations of sensing radiation before completion of transient processes was shown. At present the efficiency of the phase conjugation algorithm with account of natural oscillations of reflecting surface of acorrector is investigated. Changing the method of force application to a mirror, we are supposed to decrease the influence of transient processes on a control algorithm. As an illustration, the oscillation of the surface driven by smoothly increasing components of the vector **F** rather than by its step components is shown in Fig. 6. The significant decrease in the oscillation amplitude is observed.

REFERENCES

1. D.L. Fried and J.L. Vaughn, Appl. Opt. **31**, No. 15, 2865–2882 (1992).
2. V.P. Lukin, N.N. Maier, and B.V. Fortes, Atm. Opt. **5**, No. 12, 801–807 (1992).
3. R.K. Tyson, Opt. Eng. **29**, No. 10, 1165–1173 (1990).
4. P.A. Konyaev, V.P. Lukin, and B.V. Fortes, Opt. Am. **1**, No. 4, 71–75 (1988).
5. D.E. Novoseller, J. Opt. Soc. Am. A **5**, No. 10, 1937–1942 (1988).
6. R.J. Noll, J. Opt. Soc. Am. **66**, No. 3, 207–211 (1976).
7. N. Roddier, Opt. Eng. **29**, No. 10, 1174–1180 (1990).
8. V.P. Lukin, F.Yu. Kanev, and B.V. Fortes, Atm. Opt. **5**, No. 12, 852–854 (1992).
9. P.M. Ogibalov, *Deflection, Stability, and Oscillations of Plates* (State University, Moscow, 1958), 168 pp.
10. V.P. Kandidov, S.S. Chesnokov, and V.A. Vysloukh, *Finite–Element Method in Problems of Mechanics* (State University, Moscow, 1976), 178 pp.
11. D. Potter, *Computational Physics* [Russian translation] (Mir, Moscow, 1975), 376 pp.
12. F.Yu. Kanev, L.N. Lavrinov, and V.P. Lukin, Atmos. Oceanic Opt. **6**, No. 8, 552–558 (1993).
13. F.Yu. Kanev, V.P. Lukin, L.N. Lavrinova, and S.S. Chesnokov, Atmos. Oceanic Opt. **6**, No. 12, 844–847 (1993).